Supplementary information

for

Transient phase transition during the hydrogen evolution reaction

Yinghe Zhao,‡*[a] Haobo Li,‡[a] Ruoou Yang,‡[a] Shuxian Xie,[b] Teng Liu,[a] Pengyu Li,[a] Youwen Liu,[a] Huiqiao Li,[a] Fa Yang*[b] and Tianyou Zhai*

[a] State Key Laboratory of Materials Processing and Die & Mould Technology, School of Materials Science and Engineering, Huazhong University of Science and Technology, Wuhan, Hubei 430074, China

[b] Key Laboratory of the Ministry of Education for Advanced Catalysis Materials, College of Chemistry and Materials Science, Zhejiang Normal University, Jinhua, Zhejiang 321004, China

‡ Yinghe Zhao, Haobo Li and Ruoou Yang contributed equally to this work.

* E-mail: zhaoyh@hust.edu.cn; yangfa@zjnu.edu.cn; zhaity@hust.edu.cn

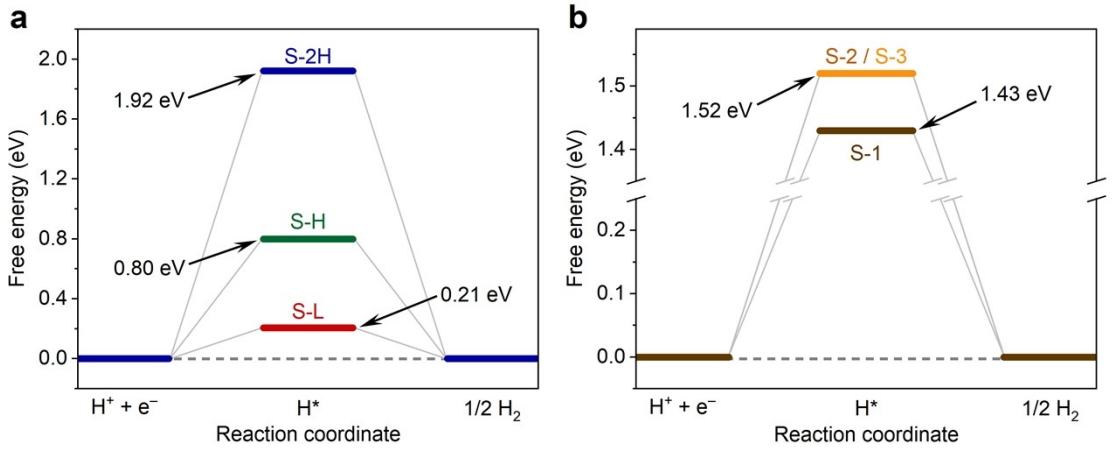

Fig. S1 (a) Free energy diagrams of the HER proceeding on 2H-MoS_2 and 1T′-MoS_2 at $U = 0$ V. S-2H represents the surface S atom of 2H-MoS_2, and S-H and S-L denote the S atoms of 1T′-MoS_2 at the higher and lower positions. The diagrams were calculated based on the 2 × 2 × 1 2H-MoS_2 and 2 × 1 × 1 1T′-MoS_2 systems using a 9 × 9 × 1 *k*-point grid. (b) Free energy diagrams of the HER proceeding on the S atoms adjacent to the vacancy (*i.e.*, S-1, S-2, and S-3) at $U = 0$ V. The positions of S-1, S-2, and S-3 relative to the vacancy are presented in Fig. 3a. The diagrams were calculated based on the 4 × 4 × 1 2H-MoS_2 system using a 5 × 5 × 1 *k*-point grid. By comparing the results in (a) and Fig. 1b and e, it can be concluded that the ΔG_H value at a 9 × 9 × 1 k-point grid is almost equal to that at a 5 × 5 × 1 k-point grid. Therefore, the 5 × 5 × 1 *k*-point grid is enough for the ΔG_H calculation. Similarly, for the 4 × 4 × 1 2H-MoS_2 system, a 3 × 3 × 1 *k*-point grid is enough for the ΔG_H calculation, as can be concluded from the comparison of the ΔG_H values in (b) and Fig. 3b.

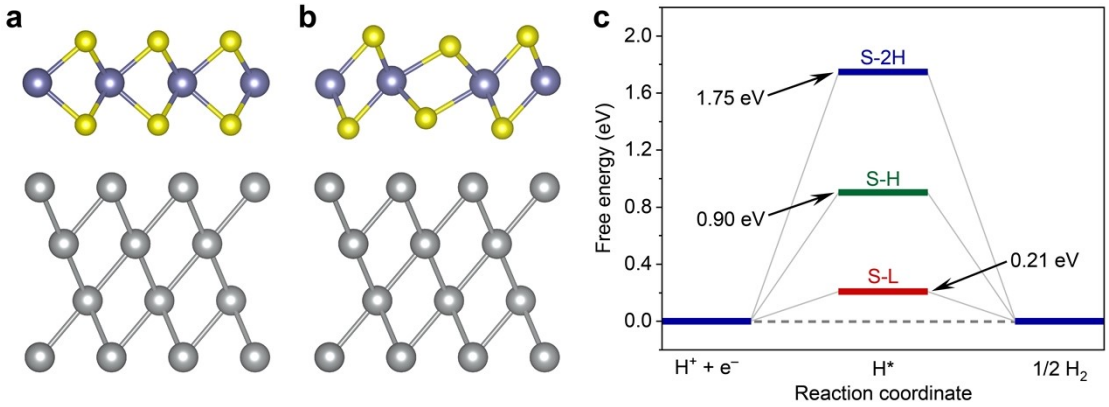

Fig. S2 (a and b) Structures of 2H-MoS_2/Ag and 1T′-MoS_2/Ag heterostructures. (c) Free energy diagrams of the HER proceeding on the surface S atom of 2H-MoS_2 (S-2H) and the surface S atoms of 1T′-MoS_2 (S-H and S-L) at $U = 0$ V. By comparing with the results in Fig. 2b and e, it can be concluded that the effect of Ag on the ΔG_H of MoS_2 is slight. Additionally, even when Ag is taken into consideration, a rather negative potential is still required to drive the S–H bonding formation on 2H-MoS_2, while a potential of ca. −0.2 V enables the S–H bonding formation on S-L of 1T′-MoS_2. The effect of Ag on the frequency of ν(S–H) is presented in Table S1. Based on the results in Fig. S2 and Table S1, it can be concluded that the 2H-to-1T′ phase transition is a plausible explanation for an unclear experimental phenomenon: the S–H bonding formation was observed on the surface when using Ag@2H-MoS_2 to catalyse the HER (*J. Am. Chem. Soc.*, 2020, **142**, 7161–7167).

Table S1 Theoretical values of the frequencies of ν(S–H) and ν(S–D) on the 2H-MoS_2/Ag heterostructure and the 1T′-MoS_2/Ag heterostructure. Mode I and Mode II represent the non-perpendicular and perpendicular adsorption modes, respectively (see Fig. 2d and e for the atomic arrangements of two modes). S-H and S-L denote the S atoms of 1T′-MoS_2 at the higher and lower positions. By comparing with the results in Fig. 2d,e, it can be concluded that Ag has a slight effect on the stretching frequency of the S–H bond. However, even when Ag is taken into consideration, the theoretical values of the frequencies of ν(S–H) and ν(S–D) on S-L are still in good agreement with the experimental values (2532 cm^{-1} and 1823 cm^{-1}, respectively; the values were obtained from the study by Chen et al. (J. Am. Chem. Soc., 2020, **142**, 7161–7167)), while the corresponding theoretical values on 2H-MoS_2 still deviate significantly from the experimental values. The effect of Ag on the ΔG_H of the surface atom is presented in Fig. S2. Based on the results in Fig. S2 and Table S1, it can be concluded that the 2H-to-1T′ phase transition is a plausible explanation for an unclear experimental phenomenon: the S–H bonding formation was observed on the surface when using Ag@2H-MoS_2 to catalyse the HER (*J. Am. Chem. Soc.*, 2020, **142**, 7161–7167).

Adsorption / Proton	2H-MoS_2		1T′-MoS_2	
	Mode I	Mode II	S-H	S-L
H (cm^{-1})	1907	2191	2448	2556
D (cm^{-1})	1364	1575	1756	1834

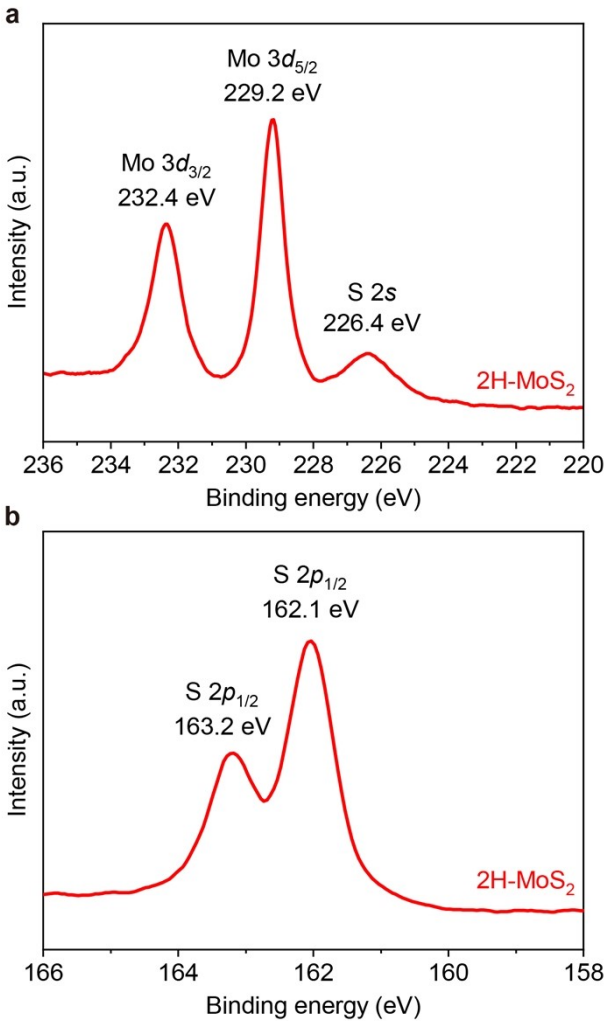

Fig. S3 XPS spectra of Mo 3*d* states and S 2*s* and 2*p* states of MoS_2 (characterised by X-ray photoelectron spectroscopy (AXIS-ULTRA DLD-600W)).

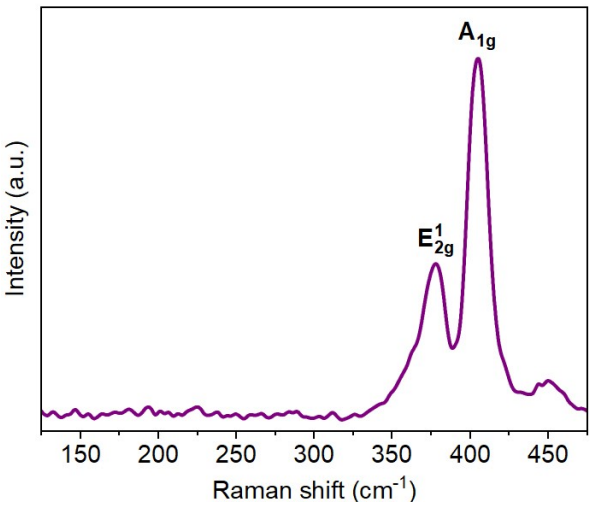

Fig. S4 Raman spectrum of MoS_2 (characterized by a confocal Raman spectroscopy (Alpha300, WITec) with 532 nm laser source).

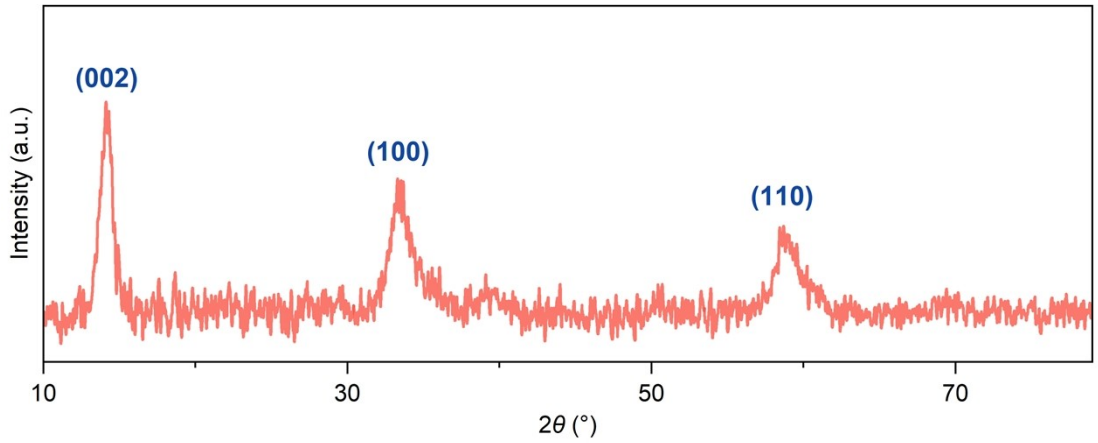

Fig. S5 XRD pattern of MoS_2 (characterised by an X-ray diffractometer (D2 PHASER, Bruker, Cu Kα, λ = 1.5405 Å)).

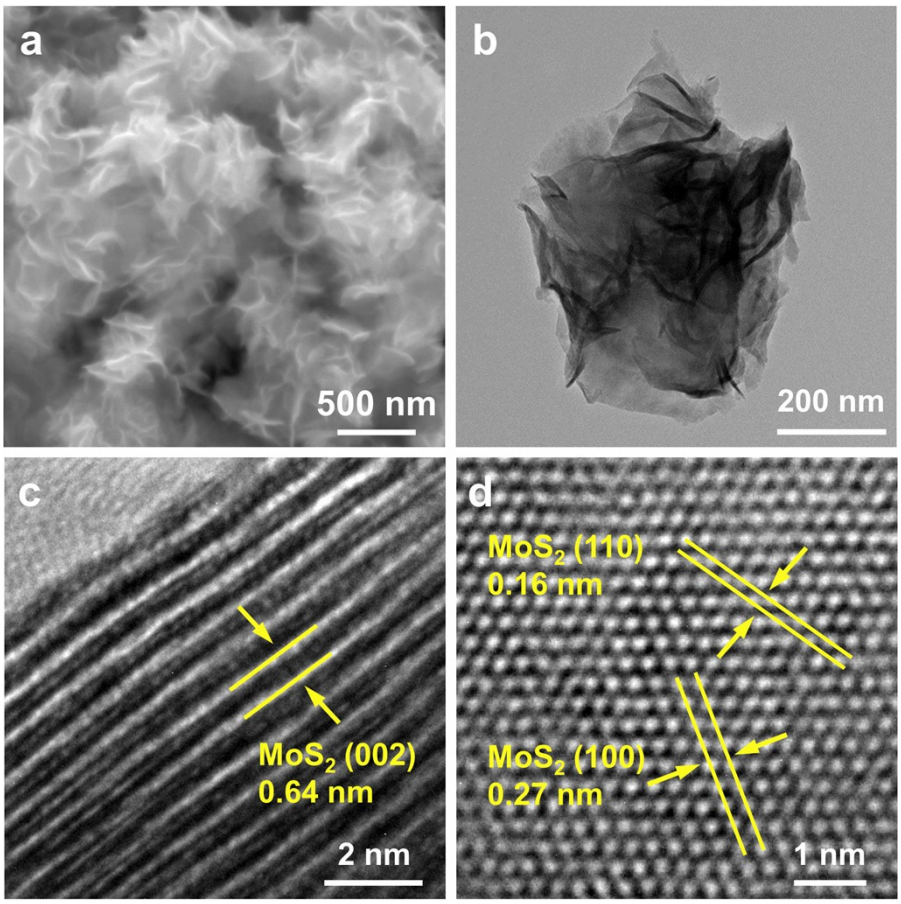

Fig. S6 (a) Scanning electron microscopy (SEM), (b) transmission electron microscopy (TEM), and (c and d) high-resolution transmission electron microscopy (HRTEM) images of MoS_2. The SEM image was obtained using a FEI quanta650 scanning electron microscope. The TEM and HRTEM images were obtained using a FEI Tecnai G2 F30 transmission electron microscope.

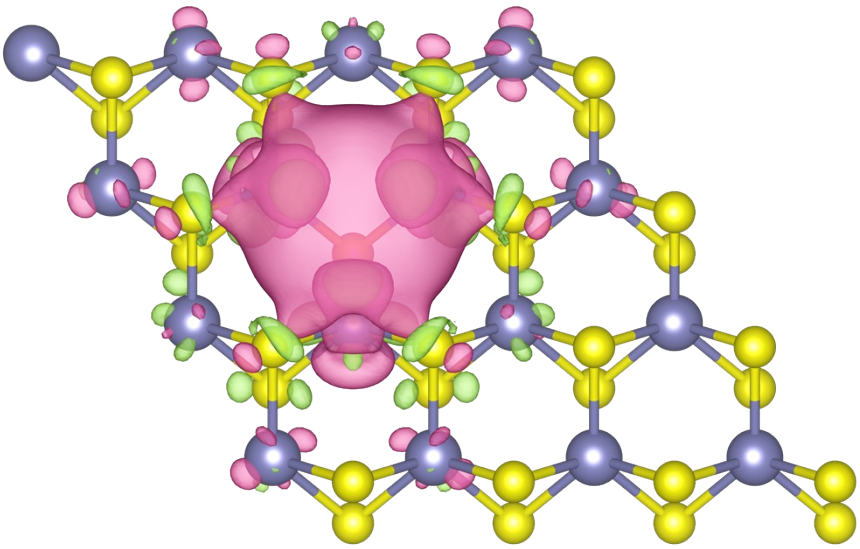

Fig. S7 Charge density difference resulting from the generation of the S-vacancy. The isosurface level is set to be 0.0006 e/Bohr^3.

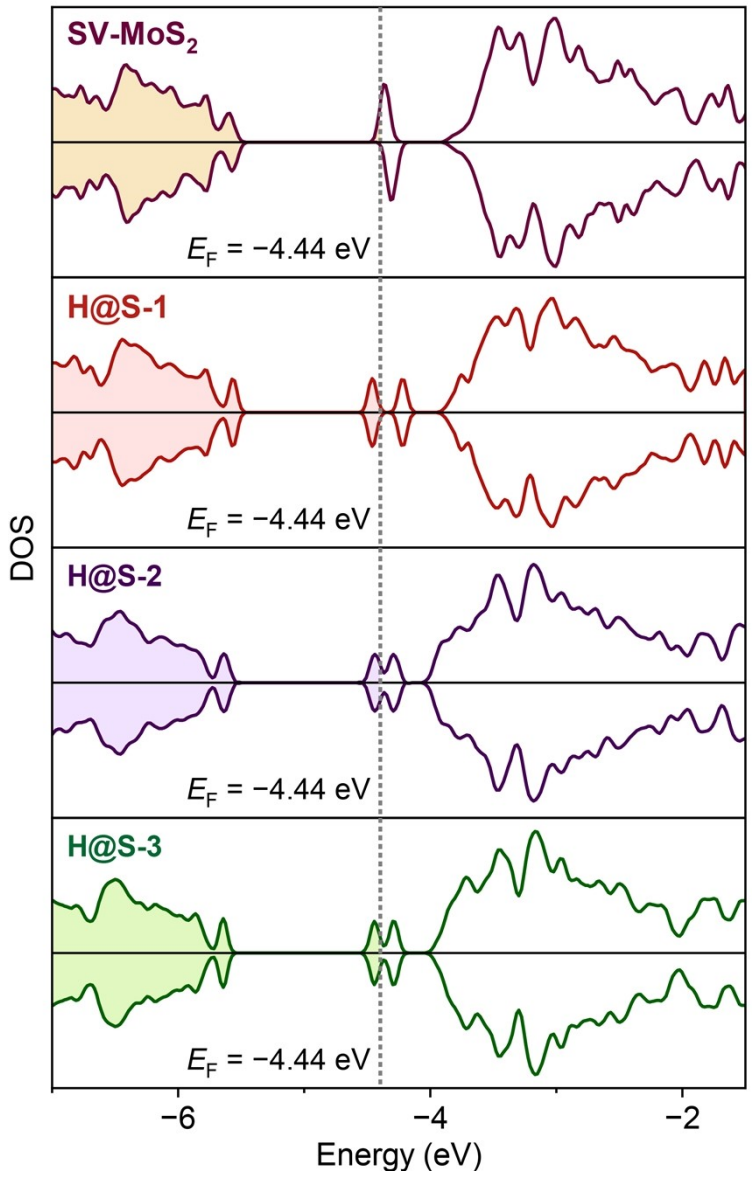

Fig. S8 Densities of states of SV-MoS_2, H@S-1, H@S-2, and H@S-3 at U = 0 V, where the Fermi level is denoted as E_F. SV-MoS_2 represents 2H-MoS_2 with a S-vacancy (Fig. 2a). H@S-1, H@S-2, and H@S-3 represent SV-MoS_2 with a H adatom on S-1, S-2, and S-3, respectively (see Fig. 3a for the meanings of S-1, S-2, and S-3).

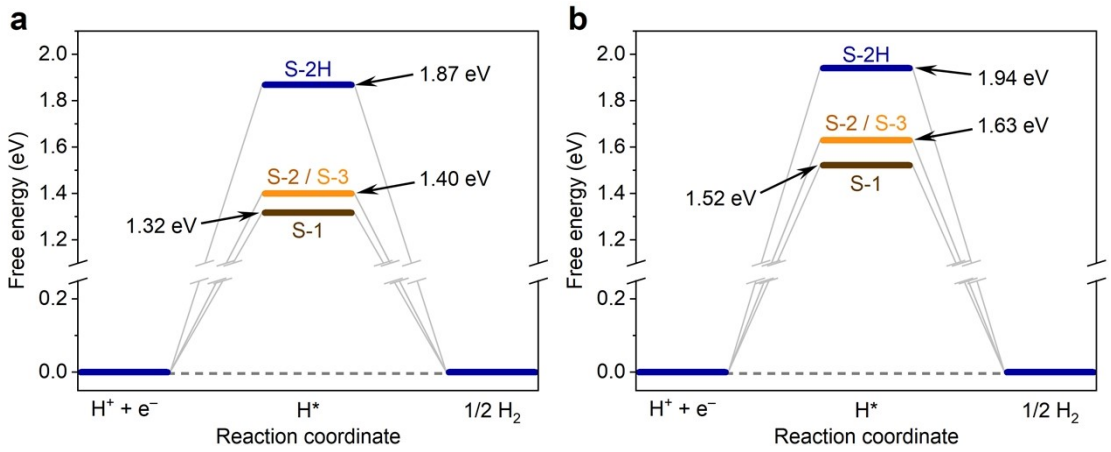

Fig. S9 Free energy diagrams of the HER proceeding on 2H-MoS_2 with (a) 1.5% tensile strain and (b) 1.5% compressive strain at $U = 0$ V. S-2H represents the surface S atom of 2H-MoS_2, and S-1, S-2, and S-3 represent the S atoms adjacent to the vacancy (see Fig. 3a for the positions of the S atoms relative to the vacancy).

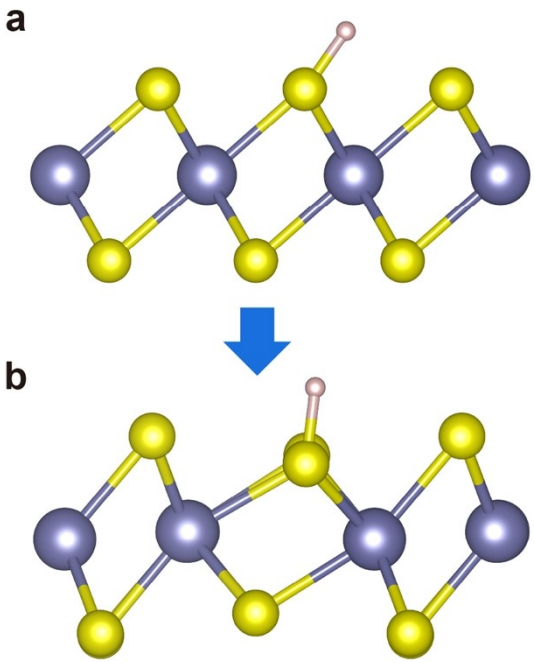

Fig. S10 H adsorption-induced phase transition from (a) 1T-MoS_2 to (b) 1T′-MoS_2.

Table S2 Theoretical values of the frequencies of ν(S–H) on the basal plane and the near-S-vacancy S atom of 2H-MoS_2 with 1.5% tensile strain and 1.5% compressive strain. Mode I and Mode II represent the non-perpendicular and perpendicular adsorption modes, respectively (see Fig. 2d and e for the difference of two modes). S-v represents the near-S-vacancy S atom. Notably, since the non-perpendicular adsorption of the H atom cannot exist stably on S-v, the non-perpendicular mode was not considered for the adsorption of the H atom on S-v.

Adsorption / Strain	Basal Plane		S-v
	Mode I	Mode II	
1.5%	1981 cm^{-1}	2039 cm^{-1}	2317 cm^{-1}
−1.5%	1924 cm^{-1}	2028 cm^{-1}	2227 cm^{-1}

Table S3 Theoretical values of the frequencies of ν(S–D) on the basal plane and the near-S-vacancy S atom of 2H-MoS_2 with 1.5% tensile strain and 1.5% compressive strain. Mode I and Mode II represent the non-perpendicular and perpendicular adsorption modes, respectively (see Fig. 2d and e for the difference of two modes). S-v represents the near-S-vacancy S atom. Notably, since the non-perpendicular adsorption of the D atom cannot exist stably on S-v, the non-perpendicular mode was not considered for the adsorption of the D atom on S-v.

Adsorption / Strain	Basal Plane		S-v
	Mode I	Mode II	
1.5%	1418 cm^{-1}	1465 cm^{-1}	1664 cm^{-1}
−1.5%	1376 cm^{-1}	1454 cm^{-1}	1598 cm^{-1}

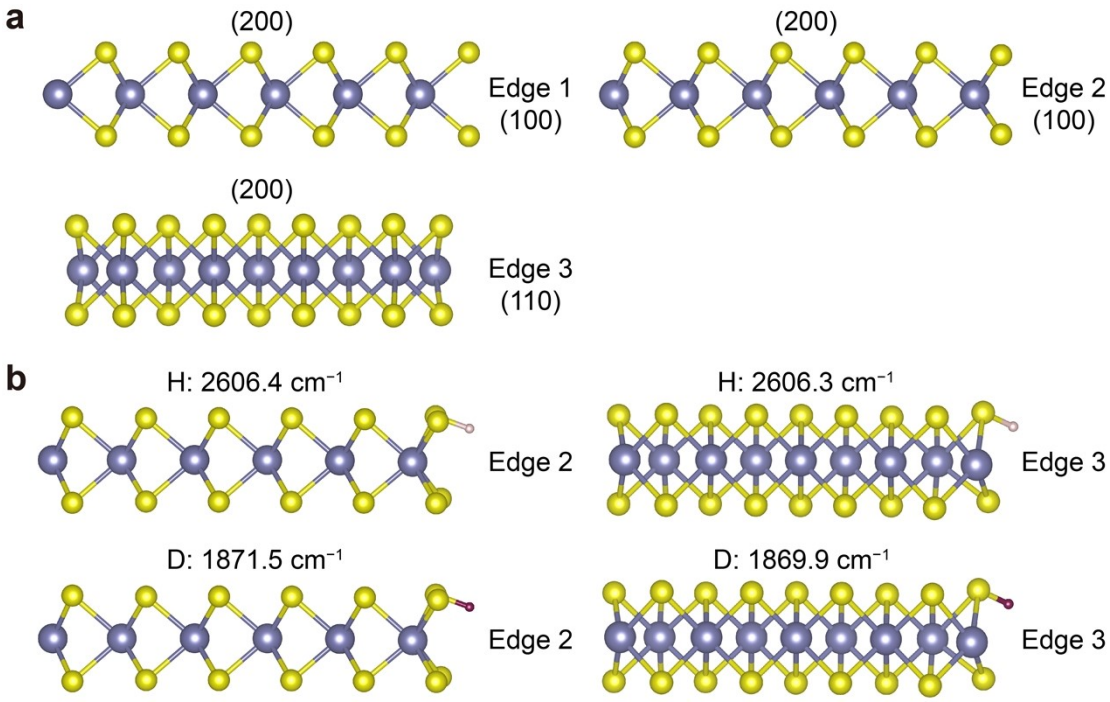

Fig. S11 (a) Edges of 2H-MoS_2 corresponding to the (100) and (110) crystal planes. It is worth emphasizing that the (200) plane corresponds to the basal plane of 2H-MoS_2. (b) Theoretical values of the frequencies of ν(S–H) and ν(S–D) on Edge 2 and Edge 3.

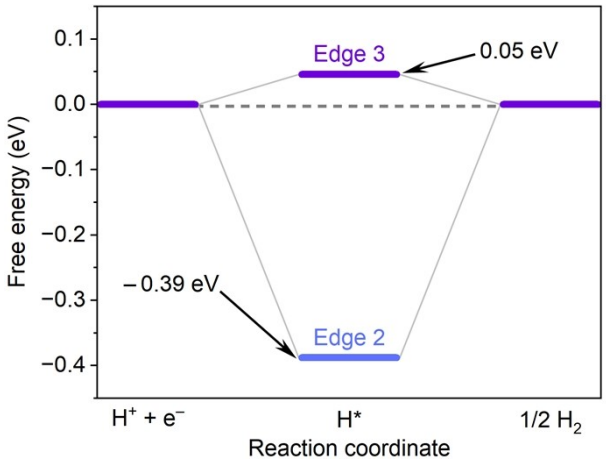

Fig. S12 Free energy diagrams of the HER proceeding on Edge 2 and Edge 3 (Fig. S11a) at $U = 0$ V.

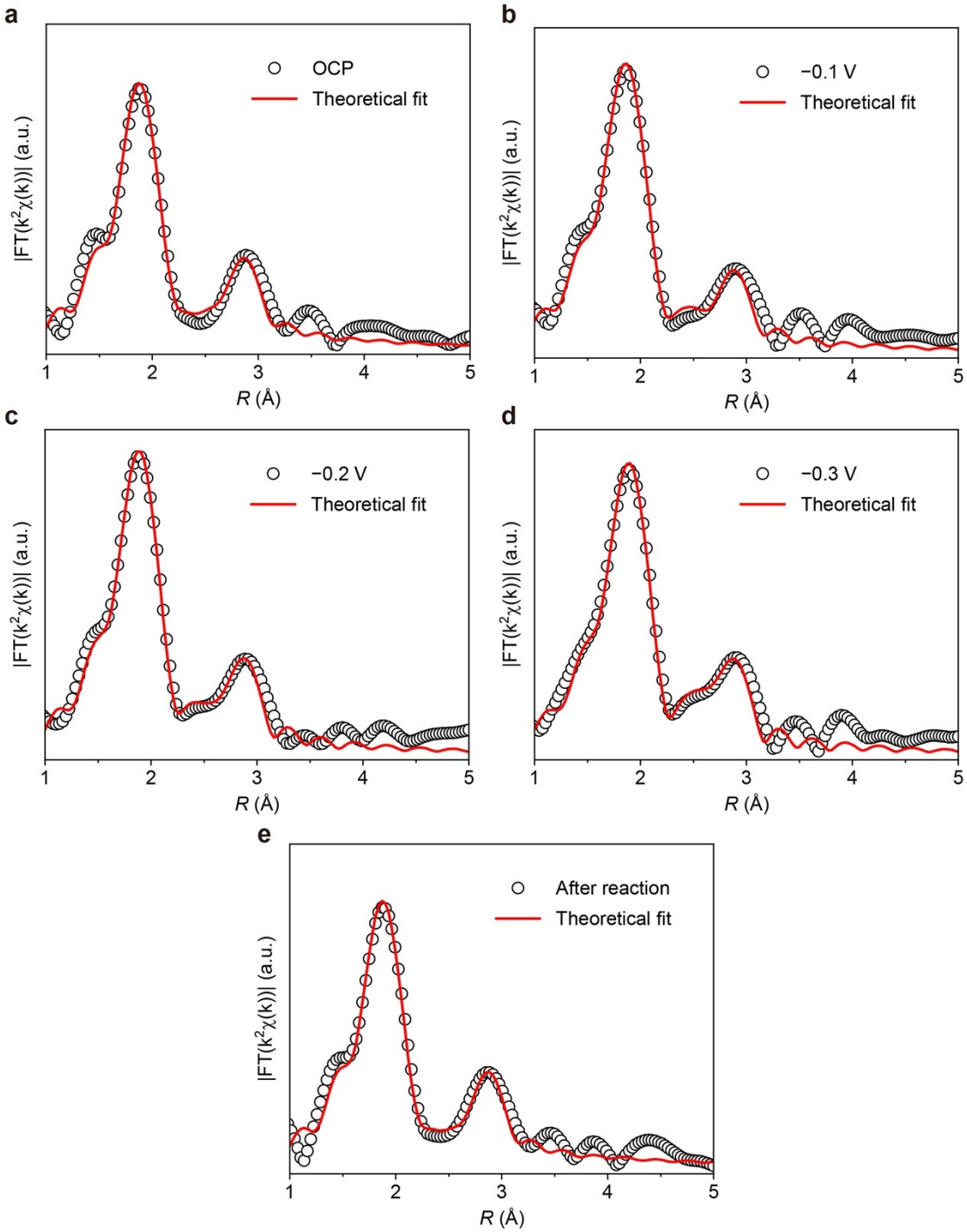

Fig. S13 Experimental and best-fitted EXAFS spectra in *R* space for MoS_2 at (a) OCP, (b) at −0.1V, (c) at −0.2 V, (d) at −0.3V, and (e) after the reaction. The peak position in the *R* space does not represent the real bond length. The real bond length can be derived by fitting the EXAFS spectra (see Table S4 for the real bond length).

Table S4 Mo K-edge EXAFS curve fitting parameters.

Sample	Shell	*N*	*D* (Å)	$\Delta\sigma^2*10^3$ (Å^2)	ΔE_0 (eV)	R-factor (%)
Mo foil	Mo-Mo1	8.0(set)	2.72±0.01	3.83±0.72	-7.8±0.8	0.3
	Mo-Mo2	6.0(set)	3.13±0.01	3.25±0.98	-7.8±0.8	
OCP	Mo-S	4.1±0.4	2.40±0.01	2.17±0.82	-0.5±0.6	1.3
	Mo-Mo	1.5±0.2	3.14±0.02	2.37±1.10	-3.7±1.8	
-0.1V	Mo-S	4.8±0.5	2.39±0.01	3.50±1.56	-0.3±0.9	1.4
	Mo-Mo	1.5±0.2	3.14±0.02	3.65±1.60	-3.6±2.6	
-0.2V	Mo-S	4.7±0.4	2.40±0.02	8.15±1.03	0.3±1.2	0.9
	Mo-Mo1	0.3±0.1	2.76±0.03	2.04±1.37	6.1±2.8	
	Mo-Mo2	1.6±0.2	3.14±0.03	8.15±1.16	-2.8±3.2	
-0.3V	Mo-S	4.9±0.5	2.40±0.02	7.87±3.66	0.9±0.9	0.1
	Mo-Mo1	0.6±0.1	2.77±0.03	6.36±5.69	6.2±6.4	
	Mo-Mo2	1.5±0.2	3.14±0.02	1.04±0.97	-2.6±2.2	
After reaction	Mo-S	4.1±0.4	2.40±0.02	2.07±0.95	-0.3±0.9	1.5
	Mo-Mo	1.5±0.2	3.14±0.03	2.64±1.10	-2.9±2.0	

N, *D*, σ^2, ΔE_0, and R-factor represent the coordination number, the distance between absorber and backscatter atoms (*i.e.*, the bond length), Debye-Waller factor to account for both thermal and structural disorders, inner potential correction, and the goodness-of-fit, respectively. The data ranges for the fitting in k-space and R-space are $2.3 \leq k$ (Å^{-1}) ≤ 12.5 and $1.2 \leq R$ (Å) ≤ 3.2, respectively. The obtained S_0^2 of Mo foil was 0.95, and it was fixed in the subsequent fitting for Mo K-edge.

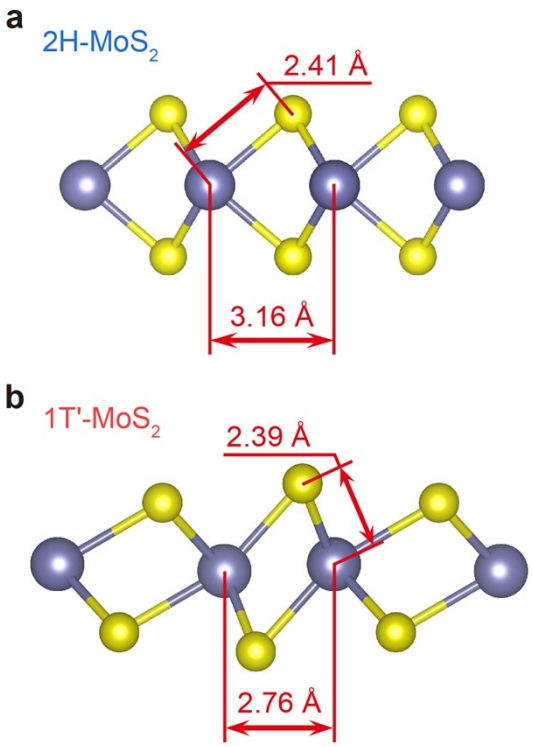

Fig. S14 (a) Theoretical lengths of the Mo–S and Mo–Mo bonds of 2H-MoS_2. (b) Theoretical lengths of the Mo–S and Mo–Mo bonds of 1T′-MoS_2. The structures of 2H-MoS_2 and 1T′-MoS_2 have been optimised through first-principles calculations.

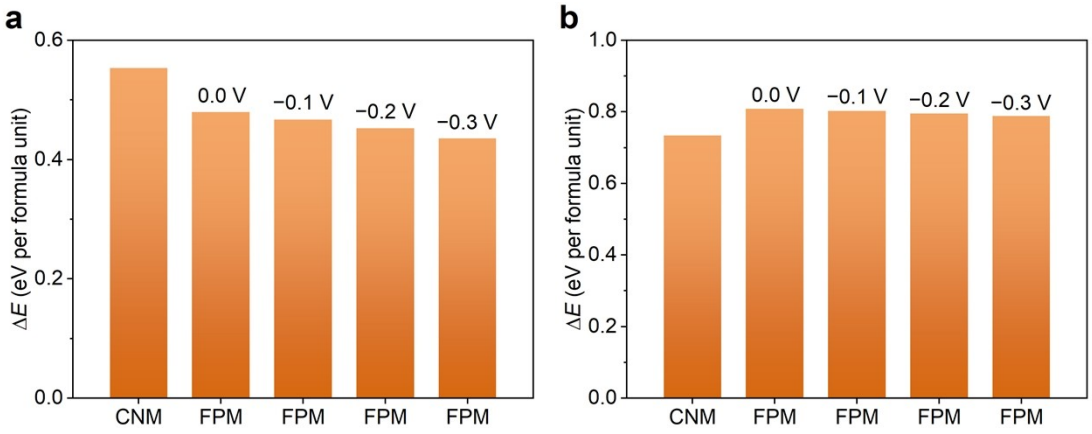

Fig. S15 Energy differences (a) between 2H-MoS_2 and 1T′-MoS_2 and (b) between 2H-MoS_2 and 1T-MoS_2. The results were calculated based on either the CNM method or the FPM method. The 1T phase transforms to the 1T′ phase with the adsorption of the H atom (Fig. S10). Therefore, there is a possibility that the 2H-to-1T phase transition first occurs and then the 1T phase is changed into the 1T′ phase by the H adatom. Comparing the results in (a) and (b), it can be concluded that the 1T′ phase exhibits higher stability compared with the 1T phase. These results show that the 2H-to-1T phase transition does not occur prior to the 2H-to-1T′ phase transition.